Magnetism in graphene due to single-atom defects: dependence on the concentration and packing geometry of defects

2009 J. Phys.: Condens. Matter 21 196002

(http://iopscience.iop.org/0953-8984/21/19/196002)

IOP Publishing Journal of Physics: Condensed Matter

J. Phys.: Condens. Matter **21** (2009) 196002 (7pp) doi:10.1088/0953-8984/21/19/196002

Magnetism in graphene due to single-atom defects: dependence on the concentration and packing geometry of defects

Ranber Singh[1,3] **and Peter Kroll**[2]

[1] Institute für Anorganische Chemie, RWTH, D-52056 Aachen, Germany
[2] Department of Chemistry and Biochemistry, University of Texas, Arlington, TX 76019, USA

Received 8 October 2008, in final form 5 February 2009
Published 7 April 2009
Online at stacks.iop.org/JPhysCM/21/196002

Abstract

The magnetism in graphene due to single-atom defects is examined by using spin-polarized density functional theory. The magnetic moment per defect due to substitutional atoms and vacancy defects is dependent on the density of defects, while that due to adatom defects is independent of the density of defects. It reduces to zero with decrease in the density of substitutional atoms. However, it increases with decrease in density of vacancies. The graphene sheet with B adatoms is nonmagnetic, but with C and N adatoms it is magnetic. The adatom defects distort the graphene sheet near the defect perpendicular to the sheet. The distortion in graphene due to C and N adatoms is significant, while the distortion due to B adatoms is very small. The vacancy and substitutional atom (B, N) defects in graphene are planar in the sense that there is in-plane displacement of C atoms near the vacancy and substitutional defects. Upon relaxation the displacement of C atoms and the formation of pentagons near the vacancy site due to Jahn–Teller distortion depends upon the density and packing geometry of vacancies.

(Some figures in this article are in colour only in the electronic version)

1. Introduction

The unconventional magnetism observed in carbon-based materials has attracted a great deal of interest in metal-free magnetic materials due to their technological advantages over metallic magnetic materials [1]. The local magnetic moments having strong long range magnetic coupling are responsible for the high-temperature magnetism observed in carbon-based materials [2]. The occurrence of high-temperature ferromagnetism in purely sp-bonded materials is a major challenge to the existing theoretical understanding of magnetic interaction mechanisms in d electron systems. A chemical or structural defect in carbon-based materials may lead to local magnetic moments due to the presence of under- or over-coordinated atoms. A number of factors, including dislocations, vacancies and impurity atoms, have been proposed which possibly give rise to the magnetism in carbon-based materials [3–12]. Graphene (a single sheet of graphite) is one such carbon-based material. Ideal graphene is nonmagnetic. However, the presence of defects induces magnetism in graphene [4, 6, 8, 13]. Defects in graphene can be created intentionally by irradiating the material with ions [2, 14]. The single-atom defects in graphene also give rise to quasi-localized states near the Fermi level [15, 16]. The fact that quasi-localized states lie at the Fermi level suggests that itinerant magnetism can be induced due to electron exchange instability [17]. Recently, the impurity and defect induced magnetism in graphitic sheets and nanotubes of boron nitride have also been reported by many authors [18–20]. Lattice distortions like cracks and large voids can induce localized states at the Fermi level which lead to the local magnetic moments in graphene [21].

The novel ways of manipulating magnetism in graphene are through vacancies, substitutional atoms and adatoms. Substitutional doping of B and N atoms can provide more control over the electronic and magnetic properties of graphene as B and N have one electron less or more than C, while they have the same atomic radius as C. The study of impurity induced magnetism in graphene is important for many reasons including: (1) the mechanism of unconventional magnetism in carbon-based systems is still not fully understood, the

[3] Present address: Max-Planck-Institut für Festkörperforschung Heisenbergstrasse 1, Stuttgart, Germany.

contributions from small element impurities like N and B cannot be excluded; (2) magnetism induced by B and N impurities along with electronic properties may be controlled by controlling the content of these impurities. Moreover, due to increasing interest in spintronic devices the magnetism in graphene has attracted more attention [22–27]. Stable and tunable magnetism in graphene will lead to many technological applications. Recently, a defective graphene phase has been predicted to be a room temperature ferromagnetic semiconductor [27]. It is also shown that the energy band gap and magnetic coupling strength can be varied by varying the defect concentration [27]. The ballistic electronic conductivity observed in graphene has also attracted a lot of attention because of its technological applications [28]. There are still many issues which need to be addressed. How does the impurity induced magnetism in graphene depend upon the concentration and packing geometry of defects? Is the impurity induced magnetism tunable by controlling the impurity defect concentration and/or the packing geometry of defects? In this paper we carried out spin-polarized density functional theory calculations on the magnetism in graphene induced by single-atom defects. Our main focus is on the dependence of magnetism on the concentration and packing geometry of defects in graphene.

2. Computational methods and models

We investigated magnetism in graphene using spin-polarized density functional theory (DFT) and the generalized gradient approximation (GGA) [29] as implemented in the Vienna *ab initio* simulation package (VASP) [30, 31]. We used projector augmented wave (PAW) pseudopotentials [32, 33] to describe the core ($1s^2$) electrons and valence electrons (($2s^2$, $2p^1$) for B, ($2s^2$, $2p^2$) for C and ($2s^2$, $2p^3$) for N). A kinetic energy cutoff of 400 eV was used to converge the total energy of our systems to within meV. The Monkhorst–Pack k-point mesh of $3 \times 3 \times 1$ (Γ point included) was used for Brillouin zone integration. The electronic smearing used in the present calculations is 0.02 which is very small and corresponds to about 232 K. The total energy and magnetic moments of model samples studied in this computational work almost converge to constant values for the kinetic energy cutoff of 400 eV and the Monkhorst–Pack k-point mesh of $3 \times 3 \times 1$ (Γ point included). The size of the supercell was varied to vary the concentration of defects in graphene. The supercells were constructed with a 10 Å vacuum gap normal to the graphene sheet so that interactions between graphene and its images are negligible. The supercells used for calculations consist of 48, 60, 80 and 100 atoms which in terms of x, y, z dimensions are defined as (12.778 00, 9.838 00, 10.000 00), (12.778 00, 12.297 56, 10.000 00), (17.034 00, 12.297 56, 10.000 00) and (21.300 00, 12.297 56, 10.000 00), respectively. All calculations were performed in the spin-unrestricted manner. The minimum of total energy was found using conjugate gradient optimization. All atoms were fully relaxed until the change in forces on the ionic displacements was below 0.01 eV $Å^{-1}$. The model systems for ideal graphene and defected graphene are shown in figure 1. We used four model systems with different sizes

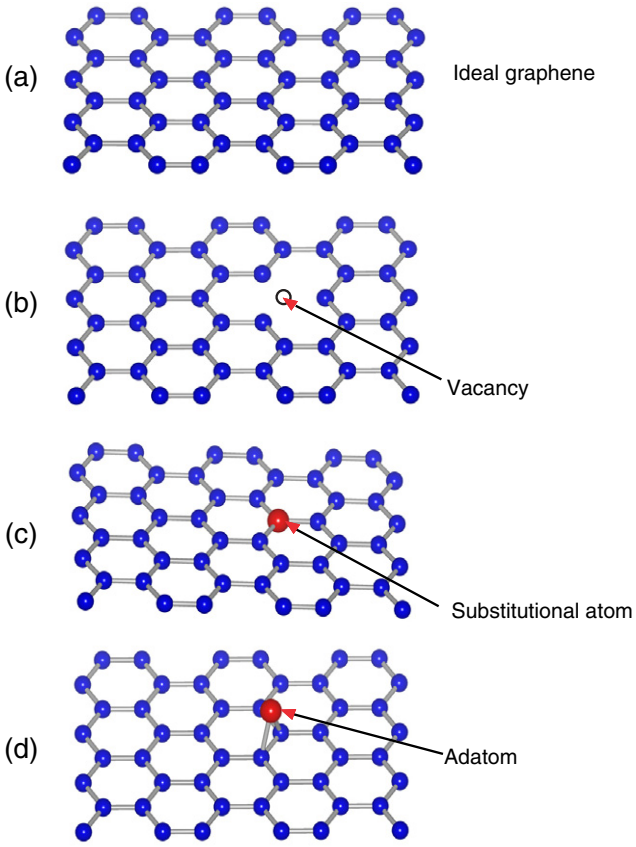

Figure 1. The model samples of (a) ideal graphene, (b) graphene with one atom vacancy, (c) graphene with one substitutional atom and (d) graphene with one adatom defect.

to study the effect of the concentration and packing geometry of defects on the magnetic properties of graphene. In 48- and 60-atom models the distance between defects is the same along the x-axis but different along the y-axis. In 80- and 100-atom models the distance between defects is the same along the y-axis but different along the x-axis. The formation energy of a single-atom vacancy (E_V) is defined as [34]

$$E_V = E_{\text{graphene+vacancy}} - \frac{N-1}{N} E_{\text{graphene}}, \tag{1}$$

while the substitutional energy (E_{sub}) [35] of substitutional defects and the adsorption energy (E_{ad}) [11] of adatom defects in model samples of defected graphene are calculated by using the following relations

$$E_{sub} = E_{\text{graphene+sub.}} - \frac{N-1}{N} E_{\text{graphene}} - E_X, \tag{2}$$

$$E_{ad} = E_{\text{graphene+adatom}} - E_{\text{graphene}} - E_X, \tag{3}$$

where N in the number of carbon atoms in the model sample of ideal graphene. E_X, E_{graphene}, $E_{\text{graphene+vacancy}}$, $E_{\text{graphene+sub.}}$ and $E_{\text{graphene+adatom}}$ are the energies of an isolated spin-polarized atom X (B, C, N), graphene, graphene + vacancy, graphene + substitutional atom and graphene + adatom systems, respectively.

Table 1. The cohesive energy of model samples of ideal graphene (E_c), and formation energies of a single-atom vacancy (E_V), the substitutional energy (E_{sub}) of a substitutional defects and adsorption energy (E_{ad}) of adatom defects in the model samples of defected graphene.

			E_{sub} (eV/atom)		E_{ad} (eV/atom)		
	E_c (eV/atom)	E_V (eV/atom)	Substitutional atom		Adatom		
No. of atoms in the model	Ideal graphene	Vacancy	B	N	C	B	N
48	8.02	7.77	5.40	4.48	1.63	1.10	0.97
60	8.02	7.80	5.37	4.44	1.65	1.06	0.98
80	8.02	7.80	5.42	4.50	1.63	0.97	0.98
100	8.02	7.80	5.45	4.50	1.60	1.05	0.93
50					1.40[a]		0.93[b]
128[c]		7.7					
	8.57[d], 8.69[e]						
Exp. [41]		7.0 ± 0.5					
Graphite (exp. [39])	7.37						

[a] Reference [51]; [b] reference [11]; [c] reference [40]; [d] reference [37]; [e] Reference [38].

3. Results and discussion

Graphene sheet is a bipartite lattice which can be viewed as two interpenetrating hexagonal sublattices of carbon atoms (say labeled as α and β) [16]. A defect created in the α sublattice breaks the symmetry between α and β sublattices giving rise to magnetic quasi-localized states in the β sublattice and vice versa [12, 36]. A number of defects are possible in graphene. In the present study, we studied only the simple single-atom defects in graphene as shown in figure 1. These defects in the model samples of graphene are considered to form a periodic two-dimensional superlattice of defects. The model samples of ideal graphene with 48, 60, 80 and 100 atoms are relaxed using the conjugate gradient optimization as mentioned in section 2. The cohesive energy of the optimized structure of each model sample of ideal graphene is given in table 1. We find that the cohesive energy of each model sample is equal to 8.02 eV/atom which is in good agreement with the previous theoretical [37, 38] and experimental results [39]. The vacancy, substitutional atom and adatom defects are created in these model samples of graphene as shown in figure 1. The created defects in model samples of defected graphene are relaxed with the same procedure as for ideal graphene. The formation energies of defects, magnetic moments and bond lengths in the optimized structures of model samples of defected graphene are given in tables 1–3. The defected graphene shows magnetism depending upon the type and concentration of defects. In the following, we will discuss in detail the results for the above mentioned three types of defects.

3.1. Vacancy defects

In this section we discuss the vacancy defects in graphene. The vacancy defects in graphene break the symmetry in the π-electron system of C atoms in graphene. This symmetry breaking gives rise to the magnetic quasi-localized states in graphene [12, 36]. The formation energies and magnetic moments of these defects in the model samples studied in this paper are given in tables 1 and 2. We find that the formation energy of vacancy defect in graphene is equal to about 7.8 eV which is good agreement with the previous theoretical [40] and experimental results [41]. As the symmetry between sublattice α and sublattice β is locally violated near the vacancy, the net magnetic moment is induced around it. The magnetic moment per defect induced in graphene due to a vacancy is found to be dependent upon the defect concentration and packing geometry of defects.

Table 2. The magnetic moment of model samples of defected graphene with single-atom defects. The vacancy defect induced magnetism in graphene depends upon the possibility of covalent bonding between the first nearest neighbors to the vacancy site. The formation of a pentagon (see figure 2(a)) saturates two of the three dangling bonds, but the remaining unsaturated bond is responsible for a magnetic moment of about 1 μ_B. In 60-atom sample models, the formation of two pentagons left two dangling bonds partially saturated and gave rise to a fractional magnetic moment of about 0.45 μ_B.

	Magnetic moment (μ_B/defect)					
		Substitutional atom		Adatom		
No. of atoms in the model	Vacancy	B	N	C	B	N
48	0.89	0.53	0.46	0.44	0.02	0.56
60	0.45	0.56	0.54	0.44	0.00	0.56
80	0.93	0.00	0.00	0.44	0.00	0.56
100	1.14	0.00	0.00	0.44	0.00	0.56
128	1.04[a]					
50				0.45[b]		0.57[c]

[a] Reference [10]; [b] reference [51]; [c] reference [11].

After removal of one C atom, each of the three neighboring C atoms now has one sp^2 dangling bond. Upon relaxation the vacancy defect undergoes Jahn–Teller distortion where the neighbor atoms to the vacancy site undergo a displacement and form weak bonds [42, 43]. The local threefold symmetry breaks down due to the Jahn–Teller distortion induced by reconstruction of the dangling bonds left after removing one C atom. This gives rise to the in-plane displacement of other C atoms near the vacancy site in the graphene lattice. The C atoms in the vicinity of the vacancy site have a C–C bond length between 1.43 and 1.44 Å. The displacement of C atoms and formation of pentagons due to the formation of weak bonds near the vacancy site depends upon the vacancy packing geometry (see figures 2(a) and (b)).

Table 3. The C–X bond lengths between substitutional atom X (X = B, N) and C atoms, the bond lengths between adatoms (C, B, N, labeled as C_{ad}, B_{ad} or N_{ad}) and C atoms (C_d) bonded to adatoms in the relaxed model structures of graphene. The C–C bond length in ideal graphene samples is equal to 1.42 Å.

	Bond length (Å)							
	Substitutional atom		Adatom					
	B	N	C_{ad}		B_{ad}		N_{ad}	
No of atoms in the model	C–B	C–N	C_d–C_{ad}	C_d–C_d	C_d–B_{ad}	C_d–C_d	C_d–N_{ad}	C_d–C_d
48	1.48	1.41	1.52	1.57	1.84	1.46	1.45	1.56
60	1.48	1.41	1.52	1.58	1.83	1.46	1.45	1.57
80	1.48	1.41	1.51	1.58	1.83	1.47	1.45	1.58
100	1.48	1.41	1.51	1.58	1.84	1.46	1.45	1.57
			1.51[a]	1.56[a]				
50							1.45[b]	1.58[b]

[a] Reference [53]; [b] reference [11].

In figures 2(a) and (b) additional bonds are shown to indicate the displacement of atoms and the formation of weak bonds after the relaxation of a vacancy defect created in graphene. In 48-, 80- and 100-atom model samples the weak bonds formed have bond lengths equal to about 2.40 Å, while in 60-atom sample models these bonds are equal to 2.42 Å. The vacancy defect induced magnetism in graphene depends upon the possibility of covalent bonding in C atoms near the vacancy site. The formation of pentagons (see figures 2(a) and (b)) partially saturates the three dangling bonds and gives rise to the fractional local magnetic moment near the vacancy site. In 48-, 80- and 100-atom model samples this fractional magnetic moment is close to 1 μ_B. However, the formation of extra bonds near the vacancy site in the 60-atom model sample gives rise to a reduced magnetic moment of about 0.45 μ_B. According to the structural dimensions of model samples as given in section 2 the vacancy defects in the 60-atom model sample form a nearly square superlattice, while in other samples vacancy defects form a rectangular superlattice. A magnetic moment of 1.15 μ_B has been predicted for the closest packing of vacancy defects [12] in a graphene sheet. Lehtinen *et al* [10] have predicted a magnetic moment of 1.04 μ_B for the ground state of vacancies in a graphite sheet.

For the vacancy defect, the total magnetic moment is determined by the contribution of localized sp^2 dangling bond states and extended quasi-localized defect states (localized p_z orbitals). Magnetism in carbon systems due to vacancies depends strongly on their concentration as well as the local bonding environment [44]. With increasing vacancy density the magnetization decreases monotonically [44]. But our results show that the magnetization induced in graphene sheets decreases non-monotonically with increasing vacancy density depending upon the packing geometry of defects. The dependence of magnetism due to vacancy defects on the concentration and packing geometry is due to the difference in the structural changes induced by the relaxation of vacancy defects in graphene. Ruderman–Kittel–Kasuya–Yosida (RKKY)-type interactions between the local magnetic moments induced at the vacancy sites are also responsible for this dependence because the RKKY interactions decay as r^{-3} where r is the distance between the defects [21]. According to the Stoner picture the magnetic ordering is driven by the exchange energy which depends upon the p_z orbitals of carbon atoms. Ferromagnetic ordering is the only possibility for the magnetism originating from the quasi-localized states induced by defects in the same sublattice because of the non-oscillating behavior of magnetization within the same sublattice and indirect RKKY interaction due to the semi-metallic properties of graphene [21].

3.2. Substitutional atom impurities

The substitutional B and N atoms are sp^2 hybridized like the C atoms in a graphitic network. If a N atom dopant does not occupy the substitutional sp^2 site in a graphitic network, it is adsorbed on the surface of the graphitic network [45, 46]. The N atom contributes two electrons, while the B atom contributes no electron to the π-electron system of C atoms. The substitutional atom and vacancy defects in graphene break the symmetry in the π-electron system of C atoms in graphene. This symmetry breaking gives rise to the magnetic quasi-localized states in graphene [12, 36]. The formation energies and magnetic moments of these defects in the model samples studied in this paper are given in tables 1 and 2. The substitutional energies for B and N substitutional defects in graphene model samples are given in table 1. The substitutional energies for B and N substitutional defects are about 5.4 and 4.5 eV, respectively. The magnetic moment per defect induced in graphene due to substitutional atoms (B, N) is about 0.5 μ_B (see table 2) in 48- and 60-atom model samples. However, it is zero in 80- and 100-atom model samples. Thus, B and N substitutional atoms induce magnetism in graphene depending upon the defect density concentration. The magnetism induced due to substitutional atoms in graphene can be understood due to the fact that a donor (acceptor) atom forms a narrow band above (below) the Fermi level (the Dirac point in graphene) [47, 48]. Here N is the donor atom and B is the acceptor atom. When the defect density is low enough the charge transfer from defect bands to π bands is complete and no magnetism is induced in graphene. However, when defect density reaches a critical density the Fermi level reaches the defect band resulting in a high density of defect states at the Fermi level. According to the Stoner criteria this leads to the development of a net

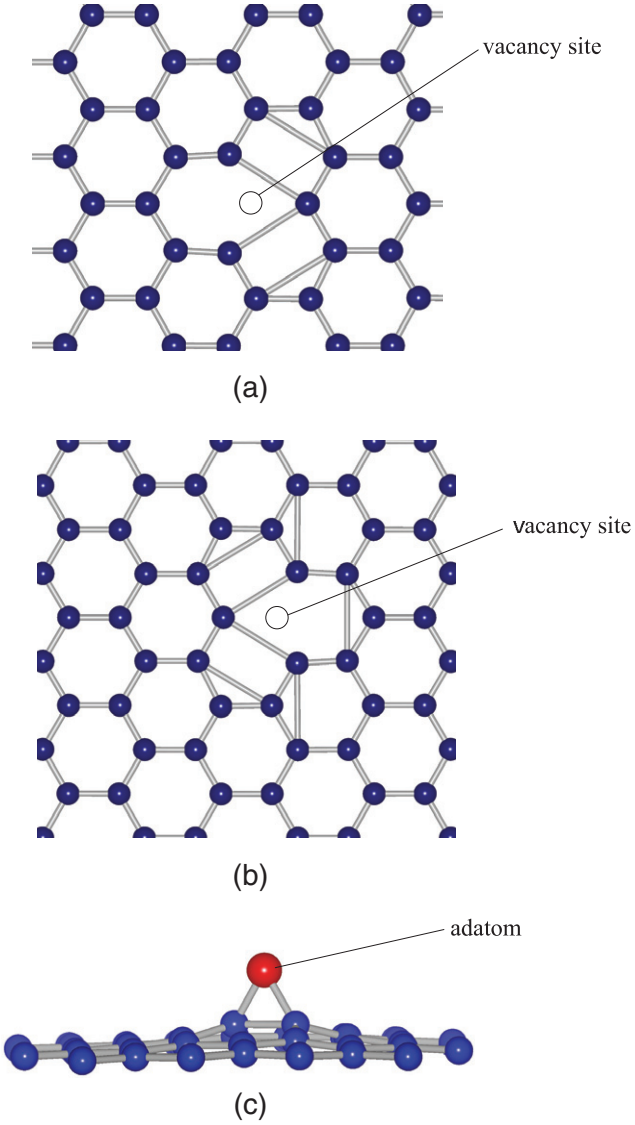

Figure 2. The relaxed structures of (a) a vacancy in 48-, 80- and 100-atom model samples, (b) a vacancy in 60-atom model sample and (c) adatom defects in the model samples of graphene. The vacancy defect is planar in the sense that displacement of atoms near the vacancy site is in plane. The extra bonds near the vacancy are shown to indicate the displacement of atoms near vacancy site and formation of weak bonds after relaxation of vacancies in graphene. In 48-, 80- and 100-atom model sample these weak bonds are about 2.40 Å, while in the 60-atom sample these are about 2.42 Å. The adatom distorts the graphene sheet perpendicular to the plane of the sheet. The distortion in the case of C and N adatoms is significant, while in the case of B adatoms it is very small.

magnetic moment in graphene [49]. The local magnetic moments having strong long range magnetic coupling are responsible for the high-temperature magnetism observed in carbon-based materials [2]. The magnetic moment of about 0.5 μ_B can be explained by the fact that the substitutional doping of a B or N atom for a C atom in graphene breaks the symmetry between α and β sublattices. When a substitutional defect is created in an α sublattice the π electron in the p_z orbital of the corresponding C atom in the β sublattice is shared between the defect state of the substitutional atom and the p_z orbital of the C atom of the β sublattice. The half electron shared by the defect state gives to a magnetic moment of about 0.5 μ_B. We also found that substitutional defects are planar in the sense that there is in-plane displacement of C atoms near the substitutional defect. In the relaxed structures of graphene, the B–C bond length is equal to 1.48 Å and the N–C bond length is equal to 1.41 Å.

3.3. Adatom impurities

There are different structures possible for adatom defects in graphene [11, 50]. But in this paper we consider only the bridgelike structures of adatoms on the graphene surface as shown in figure 1(d). This is similar to the behavior of C and O atoms on the graphene surface [51, 52]. Li *et al* have also shown that bridgelike structures of C adatoms on graphene are most stable [53]. The adsorption energies of different adatom defects in model samples studied in this paper are given in table 1. We find that the adsorption energy of a B adatom is almost the same as that of a N adatom but smaller than that of a C adatom. The calculated adsorption energies for C and N adatoms in our model samples are in quite good agreement with the previous reported results [11, 51]. The bond lengths in the relaxed model samples of defected graphene with different adatoms are given in table 3. The C, B and N adatoms are labeled as C_{ad}, B_{ad}, and N_{ad}, respectively. The C atoms bonded to adatoms are labeled as C_d. The adatom defects distort the graphene sheet perpendicular to the plane of the graphene sheet near the defect (see figure 2(c)). The bond lengths as given in table 3 show that the distortion in the case of C_{ad} and N_{ad} defects is significant, while in the case of the B_{ad} defect it is very small. The C–C_d bond length between C_d atoms and other C atoms in the graphene sheet is 1.46 Å in the case of C_{ad} and N_{ad} defects, while it is 1.43 Å for B_{ad} defects. The C_d–C_d bond length is about 1.58 Å for C_{ad}, N_{ad} defects, and about 1.46 Å for B_{ad} defects. The C_d–C_d bond length in the case of C_{ad} and N_{ad} defects is close to the C–C bond length (1.54 Å) in diamond [39]. This shows that for these defects C_d atoms become sp^3 hybridized. The C_d–C_{ad} bond is about 1.52 Å which is also close to the C–C bond length (1.54 Å) in diamond. The C_d–B_{ad} and C_d–N_{ad} bond lengths are 1.83 and 1.45 Å, respectively. The C_d–C_d, C_d–C_{ad} and C_d–N_{ad} bond lengths are consistent with the results already reported in the literature [11, 53].

Table 2 shows that magnetic moments induced due to adatoms are independent of the adatom-defect density concentration. It is 0.44 μ_B due to the C adatom and 0.56 μ_B due to the N adatom. The magnetic moment induced due to the B adatom is zero. Thus, the graphene with C and N adatoms is magnetic while that with B adatoms is nonmagnetic. The magnetic moment due to C adatoms on graphene has been explained by counting arguments that two of four valence electrons of the C adatom participate in covalent bonding with the C atoms in graphene, one electron goes to the sp^2 dangling bond of the C adatom and the fourth one is shared between the sp^2 dangling bond and the p_z orbital of the adatom [10, 51]. The p_z orbital of the C adatom is orthogonal to the π orbitals of graphene and cannot make any

bands. Consequently, the p_z orbital remains localized and spin-polarized. Thus, the half electron shared by the p_z orbital gives rise to a magnetic moment of about 0.5 μ_B. The magnetic moment of 0.44 μ_B due to the C adatom in our model samples is in good agreement with previous results of 0.44 μ_B [10]. The magnetic moment induced due to an adatom also depends upon the coupling between the π orbitals of graphene and the p orbitals of the adatom [11]. In the N adatom two valence electrons are involved in making covalent bonds with the C atoms of graphene, two electrons form a lone pair and the remaining fifth electron in the p_z orbital gives rise to a magnetic moment of 0.56 μ_B which is slightly higher than that due to the C adatom. Due to the repulsion from the lone pair, the p_z orbital of the N adatom is not completely orthogonal to the π orbitals of graphene and forms a polarized band near the Fermi level. This partially filled band gives rise to a fractional magnetic moment of 0.56 μ_B. However, in the B adatom two valence electrons are involved in covalent bonding with C atoms of graphene and a third electron is in the s orbital of the adatom which is not orthogonal to the π orbitals of graphene and forms bands with them. Consequently, B adatoms do not induce any magnetism in graphene. The magnetic moments induced due to C and N adatoms are independent of adatom-defect concentration because the magnetic moment due to C and N adatoms depends mainly upon the coupling between the π electrons and p_z unpaired electrons of adatoms. This coupling is independent of the adatom-defect concentration.

4. Conclusion

The magnetic moment per defect due to substitutional atoms (B, N) and vacancy defects is found to be dependent on the density of defects. It reduces to zero with decrease in the density of substitutional atoms, while it increases with decrease in density of vacancies. The magnetic moment per defect due to B adatoms is zero, but it is 0.44 and 0.56 μ_B due to C and N adatoms, respectively. It is also found that the adatoms distort the graphene sheet near the defect perpendicular to the sheet. The distortion in graphene due to C and N adatoms is significant, while the distortion due to B adatoms is very small. The vacancy and substitutional atom defects are planar. Upon relaxation the vacancy defect undergoes a Jahn–Teller distortion where a pentagon is formed due to the formation of a weak covalent bond between nearest neighbor atoms to the vacancy site. This gives rise to the in-plane displacement of other carbon atoms near the vacancy site in the graphene lattice. The displacement of C atoms in the vicinity of the vacancy site is between 0.01 and 0.02 Å depending upon the density and packing geometry of the vacancies.

Acknowledgments

This work is funded by the Deutsche Forschungsgemeinschaft (DFG) under project Kr-1805/8-1 (SPP 1801). We also cordially acknowledge CCC Aachen (SunFire), RWTH Aachen for providing computational facilities.

References

[1] Makarova T and Palacio F (ed) 2006 *Carbon-Based Magnetism: an Overview of Metal Free Carbon-Based Compounds and Materials* (Amsterdam: Elsevier)
[2] Esquinazi P, Spemann D, Höhne R, Setzer A, Han K-H and Butz T 2003 *Phys. Rev. Lett.* **91** 227201
[3] Fujita M, Wakabayashi K, Nakada K and Kusakabe K 1996 *J. Phys. Soc. Japan* **65** 1920
[4] Shibayama Y, Sato H, Enoki T and Endo M 2000 *Phys. Rev. Lett.* **84** 1744
[5] Khveshchenko D V 2001 *Phys. Rev. Lett.* **87** 206401
[6] Andriotis A N, Menon M, Sheetz R M and Chernozatonskii L 2003 *Phys. Rev. Lett.* **90** 026801
[7] Kusakabe K and Maruyama M 2003 *Phys. Rev.* B **67** 092406
[8] Kim Y-H, Choi J, Chang K J and Tománek D 2003 *Phys. Rev.* B **68** 125420
[9] Park N, Yoon M, Berber S, Ihm J, Osawa E and Tománek D 2003 *Phys. Rev. Lett.* **91** 237204
[10] Lehtinen P O, Foster A S, Ma Y, Krasheninnikov A V and Nieminen R M 2004 *Phys. Rev. Lett.* **93** 187202
[11] Ma Y, Foster A S, Krasheninnikov A V and Nieminen R M 2005 *Phys. Rev.* B **72** 205416
[12] Yazyev O V and Helm L 2007 *Phys. Rev.* B **75** 125408
[13] Nakada K, Fujita M, Dresselhaus G and Dresselhaus M S 1996 *Phys. Rev.* B **54** 17954
[14] Ruffieux P, Gröning O, Schwaller P, Schlapbach L and Gröning P 2000 *Phys. Rev. Lett.* **84** 4910
[15] Ruffieux P, Melle-Franco M, Gröning O, Bielmann M, Zerbetto F and Gröning P 2005 *Phys. Rev.* B **71** 153403
[16] Pereira V M, Guinea F, dos Santos J M B L, Peres N M R and Neto A H C 2006 *Phys. Rev. Lett.* **96** 036801
[17] Edwards D M and Katsnelson M I 2006 *J. Phys.: Condens. Matter* **18** 7209
[18] Wu R Q, Liu L, Peng G W and Feng Y P 2005 *Appl. Phys. Lett.* **86** 122510
[19] Si M S and Xue D S 2007 *Phys. Rev.* B **75** 193409
[20] Liu R-F and Cheng C 2007 *Phys. Rev.* B **76** 014405
[21] Vozmediano M A H, López-Sancho M P, Stauber T and Guinea F 2005 *Phys. Rev.* B **72** 155121
[22] Son Y-W, Cohen M L and Louie S G 2006 *Nature* **444** 347
[23] Ohishi M, Shiraishi M, Nouchi R, Nozaki T, Shinjo T and Suzuki Y 2007 *Japan. J. Appl. Phys.* **46** L605
[24] Tombros N, Jozsa C, Popinciuc M, Jonkman H T and van Wees B J 2007 *Nature* **448** 571
[25] Swiss Federal Institute of Technology in Lausanne 2008 Graphene holds promise for spintronics *Science Daily* 15 February
[26] Yazyev O V and Katsnelson M I 2008 *Phys. Rev. Lett.* **100** 047209
[27] Pisani L, Montanari B and Harrison N M 2008 *New J. Phys.* **10** 033002
[28] Geim A K and Novoselov K S 2007 *Nat. Mater.* **6** 183
[29] Perdew J P, Chevary J A, Vosko S H, Jackson K A, Pederson M R, Singh D J and Fiolhais C 1992 *Phys. Rev.* B **46** 6671
[30] Kresse G and Furthmüller J 1996 *Comput. Mater. Sci.* **6** 15
[31] Kresse G and Furthmüller J 1996 *Phys. Rev.* B **54** 11169
[32] Blöchl P E 1994 *Phys. Rev.* B **50** 17953
[33] Kresse G and Joubert D 1999 *Phys. Rev.* B **59** 1758
[34] Gillan M J 1989 *J. Phys.: Condens. Matter* **1** 689
[35] Yu S, Zheng W, Wen Q, Zheng B, Tian H and Jiang Q 2006 *IEEE Trans. Nanotechnol.* **5** 595
[36] Kumazaki H and Hirashima D S 2007 *J. Phys. Soc. Japan* **76** 064713
[37] Trickey S B, Müller-Plathe F, Diercksen G H F and Boettger J C 1992 *Phys. Rev.* B **45** 4460
[38] Weinert M, Wimmer E and Freeman A J 1982 *Phys. Rev.* B **26** 4571

[39] Kittel C 1996 *Introduction to Solid State Physics* (New York: Wiley)
[40] Ma Y, Lehtinen P O, Foster A S and Nieminen R M 2004 *New J. Phys.* **6** 68
[41] Thrower P A and Mayer R M 1978 *Phys. Status Solidi* a **47** 11
[42] El-Barbary A A, Telling R H, Ewels C P, Heggie M I and Briddon P R 2003 *Phys. Rev.* B **68** 144107
[43] Telling R H, Ewels C P, El-Barbary A A and Heggie M I 2003 *Nat. Mater.* **2** 333
[44] Zhang Y, Talapatra S, Kar S, Vajtai R, Nayak S K and Ajayan P M 2007 *Phys. Rev. Lett.* **99** 107201
[45] Droppa J R, Ribeiro C T M, Zanatta A R, dos Santos M C and Alvarez F 2004 *Phys. Rev.* B **69** 045405
[46] Zhao M W, Xia Y Y, Ma Y C, Ying M J, Liu X D and Mei L M 2002 *Phys. Rev.* B **66** 155403
[47] Carroll D L, Redlich P, Blase X, Charlier J-C, Curran S, Ajayan P M, Roth S and Rühle M 1998 *Phys. Rev. Lett.* **81** 2332
[48] Czerw R *et al* 2001 *Nano Lett.* **1** 457
[49] Mohan P 2003 *Magnetism in the Solid State* (Berlin: Springer)
[50] Li L, Reich S and Robertson J 2005 *Phys. Rev.* B **72** 184109
[51] Lehtinen P O, Foster A S, Ma Y, Krasheninnikov A V and Nieminen R M 2003 *Phys. Rev. Lett.* **91** 017202
[52] Sorescu D C, Jordan K D and Avouris P 2001 *J. Phys. Chem.* B **105** 11227
[53] Li L, Reich S and Robertson J 2005 *Phys. Rev.* B **72** 184109